World Journal of Engineering Research and Technology

www.wjert.org

Impact Factor: 7.029 Coden USA: WJERA4

HEAT AND MASS TRANSFER IMPACTS ON HYDROMAGNETIC FREE CONVECTIVE CHEMICALLY REACTIVE AND RADIATIVE FLOW OF HYBRID FERROFLUID OVER A NON-LINEAR STRETCHING SURFACE

Pavani Guntaka[1]*, M. Changal Raju[2]

*[1]Lecturer in Mathematics, Government Institute of Ceramic Technology, Research Scholar, JNTUA Anantapur, Andhra Pradesh, India.

[2]Professor and Head, Department of Mathematics, JNTUACE Kalikiri, Andhra Pradesh, India.

Article Received on 05/03/2025 **Article Revised on 25/03/2026** **Article Published on 04/04/2026**

***Corresponding Author**

Pavani Guntaka

Lecturer in Mathematics, Government Institute of Ceramic Technology, Research Scholar, JNTUA Anantapur, Andhra Pradesh, India.

https://doi.org/10.5281/zenodo.19435540

How to cite this Article: Pavani Guntaka[1], M. Changal Raju[2]. (2026). Heat And Mass Transfer Impacts On Hydromagnetic Free Convective Chemically Reactive And Radiative Flow Of Hybrid Ferrofluid Over a Non-Linear Stretching Surface. World Journal of Engineering Research and Technology, 12(4), 188–215.

ABSTRACT

In this work, the transport phenomena of a hybrid ferrofluid over a non-linear stretching sheet and magnetohydrodynamic (MHD) boundary layer flow are investigated. The governing partial differential equations are converted into ordinary differential equations through similarity transformations. The ODES are tackled numerically by employing the shooting strategy in conjunction with MATLAB's bvp4c solver. The study assesses the sensitivity of velocity, thermal, and concentration fields to changes in governing parameters, including the Weissenberg number, magnetic parameter, porous resistance, Darcy–Forchheimer parameter, power-law index, suction parameter, thermophoresis, radiation, Eckert number, Schmidt number and chemical reaction factor demonstrated through graphs in detail. The study concludes that magnetic, porous, Darcy-Forchheimer, Weissenberg, and suction effects reduce velocity while buoyancy and power-law behaviour increase it. Radiation, Brownian motion, thermophoresis, and the Eckert number all increase temperature fields, whereas heat absorption and a larger power-

law index decrease them. Concentration decreases with increasing Schmidt number, Brownian diffusion, thermophoresis, and chemical reactions. Skin friction and Sherwood numbers decrease under magnetic, porous, and Weissenberg influences, while solutal buoyancy and the power-law index increase them. The numerical results correlate favourably to previous literature, demonstrating the model's robustness. These findings are especially useful for improving heat transfer, energy usage, and chemical engineering applications of hybrid ferrofluids.

KEYWORDS: Hybrid ferrofluid, Convective heat and mass transfer, Thermophoresis, Brownian motion, Nonlinear stretching surface, MHD boundary layer flow.

1. Nomenclature

u_1	X-direction velocity (m/s)	u_2	**Y**-direction velocity (m/s)
$\mathbf{N_T}$	Soret effect	β_p	Permeability parameter
$\mathbf{M_0}$	Strength of Magnetic field [Tesla]	g	acceleration due to gravity [m/s²]
$\mathbf{N_B}$	Brownian diffusion	α	Chemical reactivity parameter
p	Power law(rheological) index	Γ	Relaxation time
χ	Dimensionless species concentration	θ	Dimensionless temperature
C	Species concentration	W_e	Weissenberg number
ξ	Similarity variable	$g'(\xi)$	Velocity component
$\mathbf{g_w}$	wall suction parameter	ω_t	Dimensionless thermal diffusion parameter
L	Dimensionless Magnetic flux	ω_b	Dimensionless Brownian diffusion coefficient
M	Magnetic field	u_{2_w}	Suction velocity
Cf	Skin friction coefficient	Sh	Sherwood number
E_c	Eckert number	μ	viscosity
$\mathbf{Da_p}$	Darcy-Forchheimer parameter	ρ	Fluid density
$\mathbf{R_d}$	Thermal radiation parameter	λ	Thermal conductivity
$\mathbf{P_r}$	Prandtl number	ϕ_{s1}, ϕ_{s2}	Suspended particle volume fraction
Sc_t	Schmidt number	**suffixes**	
$\mathbf{C_p}$	Heat capacity at constant pressure	Hnf	Hybrid ferrofluid
$\mathbf{G_r}$	Thermal buoyancy parameter	fer	Ferro nanofluid
$\mathbf{G_m}$	Solutal buoyancy parameter	fl	Primary fluid
$\mathbf{Q_1}$	Heat source parameter	s_1, s_2	Ferro-nanoparticles

INTRODUCTION

Examining the flow dynamics of MHD of electrically conductive fluids over stretching surfaces generated significant interest because of its significance in a variety of industrial and technical procedures, including polymer extrusion, heat dissipation in metals, solar energy systems, nuclear reactors, and biomedicine. Magnetic fields, viscous dissipation, Lorentz forces and buoyancy-driven motion have a significant effect on the fluid domain's velocity, temperature, and concentration profiles.

Javaherdeh et al.[1] examined a steady MHD flow via a plate that moves vertically within a porous medium. Through the use of a finite difference technique, they demonstrated how velocity, temperature, concentration, and both the Nusselt and mass transfer coefficient are heavily influenced by the controlling factors like porosity, magnetic field, and power-law exponents. Zigta[2] theoretically analysed unsteady MHD blood flow in a stretched permeable channel, considering the influence of heat radiation and chemical reactivity. According to the study, blood velocity rises with unsteadiness and permeability, while temperature rises with greater Hartmann and Prandtl numbers. In contrast, higher Schmidt number and stronger chemical reactivity cause the concentration to drop. Seth et al.[3] investigated the time-dependent heat flux, mass transfer and unstable heat-generating hydromagnetic natural convection motion of an incompressible, viscous, conducting fluid adjacent to an infinitely extended vertical flat plate that moves impulsively. The experiment also explored the contribution of an angled magnetic flux when there was a chemical reaction occurring in the medium. Nasir et al.[3] carried out an extensive numerical analysis of magnetohydrodynamic flow with chemical reaction via a permeable plate using the generalized heat conduction model of Cattaneo–Christov. A finite difference approach was used to solve the governing PDEs expressed in dimensionless variables. Their investigation showed that the employed model considerably modifies the dynamics of the temperature boundary layer. Mohamed[4] investigated mass transfer and MHD heat convection over a permeable vertical plate of semi-infinite extent immersed within a permeable material, considering the impacts of homogeneous chemical processes and thermal radiation. Cham et al.[5] carried out a comprehensive simulation study of unsteady Magnetohydrodynamics thermal convection in a porous cavity. Their research investigated the ways in which buoyancy-driven forces, the permeability of the porous material, and the strength of the magnetic field control flow circulation patterns and thermal properties. A finite-volume numerical method was used to run the simulations.

Nanofluids, prepared by blending nanoparticles into traditional base fluids, have gotten a lot of interest as a new way to improve heat and mass transfer properties. This is because nanotechnology is moving so quickly. A next-generation development in recent years has been the idea of a base fluid is mixed with two or more different kinds of nanoparticles to create hybrid nanofluids. These fluids have improved thermophysical characteristics that outperform those of traditional nanofluids due to the synergistic reactions among heterogeneous nanoparticles, making them extremely effective working medium for a variety of industrial and technical applications.

According to Khan and co-authors[6] examined the motion of a Williamson type nanofluid with varying viscosity & angled Lorentz force across a nonlinearly stretched surface. For heat and concentration boundary layers, stronger magnetic fields were better, whereas higher Williamson parameters reduced velocity. The three-dimensional Magnetohydrodynamic transport of a non-Newtonian nanofluid over a stretched surface has been examined by Akbar et al.,[7] taking into account thermal stratification and varying fluid characteristics. To obtain numerical solutions, the Runge–Kutta scheme was employed. The findings demonstrated that changes in viscous resistance and ability to conduct heat have a significant impact on thermal transfer characteristics as well as flow behaviour. Prabakar Reddy et al.[8] study the unstable magneto-fluid motion of a radiating, chemically reactive fluid around a vertical permeable plate with viscous contact. It is examined how key variables affect the behaviour of fluid flow. Unlike radiative absorption of heat and magnetic fields, buoyancy increases flow. It is discovered that when the rates of chemical reactions increase, the properties of heat and mass transmission show a consistent decline. Mami et al.[9] explored the characteristics of nanofluid combined convection within a porous media with magnetic along a semi-infinite stretching surface under the influence of chemical reactions. They found that while higher chemical reaction rates increase thermal and solutal transport, an intensified magnetic flux decreases these processes. Santhi et al.[10] investigated hybrid nanofluid behaviour across a stretchable surface while taking thermal radiation, fluid slip at the wall, suction and chemical reactions. The dimensionless system of equations was tackled with FEM employing a water-based TiO_2–Al_2O_3 hybrid nanofluid, demonstrating how these factors affect flow and heat transmission properties. Khan et al.[11] studied 2-phase convection of heat in a Jeffrey fluid with scattered dust particles trapped between two infinitely parallel vertical plates. The relationship between heat transport and the fluid-particulate matter interaction was emphasized. Using the shooting methodology in conjunction with the Runge–Kutta method,

nonlinear ODEs solved numerically. Sekhar et al.[12] carried out the study using the Buongiorno model on casson nanofluid motion over a slanted stretched surface when a magnetic field was present. In order to show how radiation, heat absorption, and cross-diffusion effects (Dufour and Soret numbers) interact to affect momentum, temperature, and concentration fields, they took these factors into consideration. Khan et al.[13] studied magnetohydrodynamic tangent-hyperbolic nanofluid motion along deforming surfaces, Brownian motion and thermophoresis increase temperature, whereas Weissenberg and Hartmann numbers slow down motion. Their results also show that as nanoparticle properties change, there is a decrease in heat transfer and an increase in the mass transfer coefficient. Kotnurkar et al.[14] studied the behaviour of blood inspired nanofluid embedded with iron oxide, silver, and zinc nanoparticles through a porous media under the combined effects of chemical reactions and an external magnetic field were present. By using the Homotopy Perturbation Method, they demonstrated that while higher activation energy increases both temperature and concentration, magnetic field strength decreases both. Mahmood et al.[15] used non uniform viscosity and thermal diffusion property that vary with temperature, along with slip at the boundary to numerically study heat transfer in radiative movement of hybrid nanofluid along a porous-embedded surface with instability. Their findings revealed how much differences in thermal properties and radiation impacts. To examine improved heat transfer, Madkhali et al.[16] numerically investigated MHD fluid flow of a cross-rheological fluid including ternary hybrid nanoparticles. They demonstrated using FEM that ternary nanoparticles significantly raise the Nusselt number and thermal layer thickness. Aisha Alqahtani et al.[17] examined the impacts of magnetic dipole, Darcy–Forchheimer drag, chemical interaction, and activation energy when examining trihybrid Carreau–Yasuda nanofluid flow over a vertical surface with MWCNTs, Zn&Cu nanoparticles dispersed in ethylene glycol. According to their findings, thermal transport is improved by viscous dissipation and heat creation, whereas magnetic dipoles greatly increase energy transfer while decreasing velocity. Elboughdiri et al.[18] investigated trihybrid nanofluid's 3D MHD flow across a thermally laminated surface numerically, by taking Dufour, Soret, and Stephan blowing effects into account. A framework for improving transport efficiency in MHD trihybrid nanofluids with cross-diffusion was suggested by them using the finite difference approach. Ahmad et al.[19] examined nanofluid hybrid flows involving activation energy using Hall current and ion slip effects. They demonstrated that because activation energy is highly dependent on temperature gradients, it reduces species concentration by reducing the controlling PDEs to nonlinear ODEs.

The inclusion of ferroparticles to hybrid ferrofluids attracts a lot of study interest since it not only increases the fluid's magnetic responsiveness but also significantly boosts its thermal conductivity and total heat transfer capacity. For advanced energy, cooling, and transportation applications, hybrid ferrofluids are positioned as very adaptable media due to their unique mix of magnetic and thermophysical improvements.

Dzhuraev et al.[20] examined ferrofluids formulated with transformer oil and found that their thermal conductivity, diffusivity, and heat capacity vary significantly with changes in particle loading and external magnetic field intensity. These results underline the importance held by magnetothermal effects for enhancing the functional performance of ferrofluids for technological applications. According to Mahmood et al.,[21] an IBRNN model trained with MATLAB's bvp4c aided their analysis of tetra hybrid nanofluid flow with varying electrical conductivity and viscosity using the Runge-Kutta-Fehlberg 45 and shooting methods. They discovered an increase in heat transfer of up to 0.82% when mass suction, Joule heating, and velocity slip were taken into account, emphasizing implications for aerospace thermal systems. Mahmood et al.[22] examined the dynamics of Al_2O_3–Cu/water hybrid nanofluid along a horizontally shrinking surface in a Darcy–Forchheimer permeable medium, considering slip effects, radiation, joule heating and changing viscosity. They discovered that while nanoparticle concentration and thermal conductivity enhances velocity and thermal field, thermal slip and larger Prandtl numbers decrease temperature using similarity transformations via the RK4 shooting technique. Alkasasbeh[23] used the Chebyshev differential quadrature method to evaluate Casson hybrid nanofluid motion along a vertically expanded surface under an electromagnetic flux. According to the study, a stronger magnetic field lowers the temperature. Wahid et al.[24] explored an analysis of a hybrid nanofluid flow with radiation effect was conducted on a permeable flat plate using alumina-copper nanoparticles distributed in water. Higher radiation and magnetic characteristics, as well as lower copper content, were shown to improve thermal transport while avoiding boundary layer detachment. Yashkun et al.[25] examined the MHD boundary layer flow of a Cu–AlO_3/H_2O hybrid nanofluid across a stretching/shrinking sheet with varying viscosity, suction, and radiation effects. As compared to Cu/H2O nanofluid, the results demonstrated improved heat transmission, with suction raising the local Nusselt number and skin friction. Sharma et al.[26] examined temperature-dependent viscosity, Brownian motion, and thermophoresis while examining the unsteady Von-Kármán flow of water-based ferrofluids (FeO_4, Mn–$ZnFeO_4$) over a rotating disk. They discovered that Mn–$ZnFe_2O_4$ increased radial

velocity and Fe_3O_4 improved thermal conductivity and decreased thermal boundary thickness during FHD interaction using similarity transformations and the BVP Midrich approach in Maple. Anantha Kumar et al.[27] investigated the behaviour of hybrid ferrofluids (FeO_4–$CoFeO_4$/water–EG) in liquid film flow influenced by thermal radiation was investigated by According to their findings, controlling factors strongly influence the temperature and velocity distributions, and hybrid ferrofluids transport heat more effectively than regular ferrofluids. With a nonuniform magnetic flux, Magdy et al.[28] examined heat transmission through ferrofluid flow on an unstable stretched sheet. The ODEs are solved using the Homotopy Perturbation Method, which also looked at how magneto-thermomechanical factors affected temperature, velocity and shear stress. According to this research, a stronger ferrohydrodynamic interaction raises temperature and velocity.

In addition to hybridization's benefits, non-Newtonian effects have a big impact on fluid motion and transfer behaviour. Non-Newtonian fluids exhibit shear-dependent rheology and viscoelasticity, which changes velocity profiles, boundary layer development, and energy transport in contrast to Newtonian fluids with constant viscosity. These effects enhance the interplay between external forces and fluid microstructure impacting heat and mass transport's overall performance when paired with nanoparticle suspensions.

Alharbi et al.[29] examined thermal transport characteristics of a hybrid Williamson nanofluid in the presence of Hall current with convective boundary conditions. By adding hybrid nanoparticles, the fluid's thermal performance was greatly improved. Reddy et al.[30] used the Buongiorno model with activation energy and nanoparticle dynamics to investigate Williamson nanofluid flow with magnetic effects past a wedge.

Higher activation energy and magnetic field intensity improved thermal and solutal boundary layers, but the Williamson parameter decreased flow velocity because of shear-thinning. Nadeem et al.[31] employed the HAM Method to examine boundary layer characteristics of a pseudoplastic Williamson fluid in 2D across a stretched surface. The study confirmed that increasing the Williamson fluid parameter slows fluid motion. Abbas et al.[32] investigated the influence of slip, suction/injection, along with thermal radiation effects on tangent-hyperbolic nanofluid motion across a stretching surface. They discovered that while nanoparticle effects have a major impact on heat transfer, velocity decreases with increasing suction, slip, and power-law parameters using boundary-layer modeling, similarity transformations, and the numerical shooting technique. Using radiation along with heat absorption/source, Jagadeesh

&Reddy[33] studied 3D Williamson nanofluid flow on a linearly stretched sheet. The governing ODEs were numerically solved with the shooting technique. As a result of shear-thinning effects, the Williamson parameter eases flow resistance by lowering shear rate at the surface. Hayat et al.[34] investigated transient behaviour of Williamson fluid across a deforming surface with Dufour, Soret, radiative heat transfer and viscous dissipation. For the purpose of solving time-dependent equations numerically, they were converted to nonlinear ODEs via similarity transformations. The findings demonstrated that coupled heat–mass diffusion in non-Newtonian flows is highlighted by thermal and concentration biot numbers, which dramatically increase temperature and species count.

These studies highlight how crucial ferroparticles and magnetic field arrangement are in regulating hybrid nanofluid dynamics. Various physical processes, such as the resistance of porous media, suction and injection procedures, thermophoretic and Brownian particle motion, internal heat generation or absorption and chemical reactions greatly affect the characteristics of fluid dynamics. These mechanisms, which can operate alone or in combination, complexly control mass transport, thermal energy distribution, and momentum transfer, determining how well fluid systems function overall in practical engineering and industrial settings.

A study by Rafique et al.[35] investigated heat transport in Casson nanofluids, such as SWCNTs and MWCNTs, using a sliding permeable plate and nonlinear radiation. They found that MWCNTs provide excellent heat transfer, with radiation and viscosity diminishing it and Prandtl number, Casson parameter, and nanoparticle concentration boosting it. It did this by using RK-IV with similarity transformations and the shot method. Vijay et al.[36] evaluated the transport phenomena of FC-72 magnetic nanofluid with radiation, viscous dissipation, and viscosity changes between two rotating stretchable disks. While temperature and nanoparticle concentration increase with Reynolds number, higher viscosity decreases horizontal velocity toward the bottom disk, according to similarity transformations with HAM in Mathematica. Mishra et al.[37] studied the flow behaviour and heat transfer characteristics of a hybrid nanofluid ($ZrO_2 + Fe_3O_4$) based on motor oil over a sheet in a magnetic field. Hen findings were combined with ANN predictions, the SQLM solution demonstrated good accuracy for drag and Nusselt numbers. The flow of ferrohydrodynamic nanofluids within the gap of co-rotating porous disks considering radiative heat transfer and geothermal viscosity was studied by Sharma et al.[38] Solving using BVP Midrich in Maple,

they found that skin friction is affected, viscosity variations lower horizontal velocity but raise vertical velocity, and larger Darcy numbers lower temperature. Over an infinite moving vertical plate, Arulmozhi et al.[39] investigated MHD free convection of nanofluid under chemical reactions and radiation. They demonstrated through intricate graphs how different parameters affect temperature, velocity, and species concentration using perturbation techniques. Rafique et al.[40] examined Joule heating, entropy generation, thermal stratification, and changing viscosity when analyzing an MHD ternary nanofluid (AlO_3–Cu–TiO_2/H_2O) over a stretching disk. The results from bvp4c demonstrated that ternary nanofluids can enhance heat transmission by up to 38.05%. Under varying viscosity, temperature increases and velocity decreases, while radiation and Eckert number decrease Bejan and Nusselt numbers.

The combined impacts of ferro-nanoparticles, hybrid nanofluid interactions, non-Newtonian behaviour, MHD effects, porous media, and unsteady/non-linear stretching surfaces have not been thoroughly investigated despite significant advancements. The current study fills this gap by examining the simultaneous impact of a heat source, Brownian motion, suction, thermophoresis, magnetic flux and chemical reactions influencing the thermal transport, solutal concentration profile and flow properties of a ferrofluid across a nonlinear stretching surface situated in a porous medium. MATLAB's bvp4c solver is used to solve the PDEs that characterize the flow behaviour numerically once they are reduced to nonlinear ODEs with the application of similarity transformations. The graphs demonstrate the dependence of velocity, temperature, and concentration profiles on the controlling parameters. For ferrofluid-related industrial processes, energy systems, and thermal management, this work has valuable implications.

Mathematical modelling

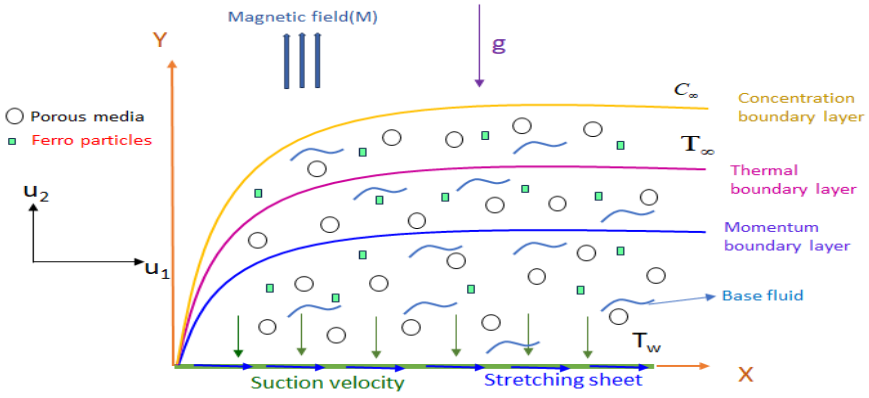

Figure 1: Detailed spatial configuration of the problem

The present model deals with steady-state dynamics of a ferrofluid across a nonlinearly stretching horizontal stretching surface embedded in a porous medium, in the presence of thermal radiation, viscous dissipation, Brownian diffusion, thermophoresis, and a non-uniform heat source. Where the sheet is aligned along the X-axis and the Y-axis is perpendicular to it, the flow is confined to the region above the sheet (Y>0) and is driven by the stretching motion of the stretching surface, characterized by a hyperbolic tangent velocity profile. The stretching velocity is assumed to vary nonlinearly along the sheet as observed in Figure1. The system is subjected to a transverse magnetic field M ($M = M_0 x^{-\frac{2}{3}}$) aligned with the Y-direction, while water is taken as the base fluid containing suspended ferro-particles. The sheet is porous, permitting suction near wall.

The concentration and thermal fields are modelled to capture heat and mass transfer phenomena. The effect of thermal radiation are incorporated via a radiative flux term, while chemical reactions occurring within the medium are described by a reaction rate parameter K. A porous media makes it easier for the ferrofluid to flow, which is represented using Darcy's law, accounting for the resistive effects of the porous structure. Additionally, the Darcy–Forchheimer extension is included.

Given aforementioned presumptions, Momentum, Species concentration and Temperature equations of hybrid ferrofluid flow model is developed by applying above-mentioned constraints, Mathematical equations (Khan et al. [15]) of flow of hybrid nanofluid are

$$\frac{\partial u_1}{\partial X} + \frac{\partial u_2}{\partial Y} = 0, \tag{1}$$

$$u_1 \frac{\partial u_1}{\partial X} + u_2 \frac{\partial u_1}{\partial Y} = g\beta\left(\mathrm{T} - \mathrm{T}_\infty\right) + g\beta^*\left(C - C_\infty\right) - \frac{\zeta_f}{\sqrt{K}} u_1^{\,2} - \frac{\mu_{Hnf}}{\rho_{Hnf} K} u_1 + \frac{\mu_{Hnf}}{\rho_{Hnf}}\left[\left(1-p\right)\frac{\partial^2 u_1}{\partial Y^2} + \sqrt{2}\, p\Gamma \frac{\partial u_1}{\partial Y}\frac{\partial^2 u_1}{\partial Y^2}\right] - \frac{\sigma_{Hnf} M^2}{\rho_{Hnf}} u_1, \tag{2}$$

$$u_1 \frac{\partial C}{\partial X} + u_2 \frac{\partial C}{\partial Y} = -K\left(C - C_\infty\right) + \frac{N_T}{\mathrm{T}_\infty}\frac{\partial^2 \mathrm{T}}{\partial Y^2} + N_B \frac{\partial^2 C}{\partial Y^2}, \tag{3}$$

$$u_1 \frac{\partial \mathrm{T}}{\partial X} + u_2 \frac{\partial \mathrm{T}}{\partial Y} = \frac{1}{\left(\rho C_p\right)_{Hnf}} \frac{\partial}{\partial Y}\left(\kappa \frac{\partial \mathrm{T}}{\partial Y}\right) + \frac{\mu_{Hnf}}{\left(\rho C_p\right)_{Hnf}}\left[\left(1-p\right)\left(\frac{\partial u_1}{\partial Y}\right)^2 + \frac{p\Gamma}{2}\left(\frac{\partial u_1}{\partial Y}\right)^3\right] - \frac{1}{\left(\rho C_p\right)_{Hnf}} \frac{16\sigma^* \mathrm{T}_\infty^3}{3k^*} + \tau\left[N_B \frac{\partial C}{\partial Y}\frac{\partial \mathrm{T}}{\partial Y} + \frac{N_T}{\mathrm{T}_\infty}\left(\frac{\partial \mathrm{T}}{\partial Y}\right)^2\right] + \frac{1}{\left(\rho C_p\right)_{Hnf}} Q\left(\mathrm{T} - \mathrm{T}_\infty\right) \tag{4}$$

The applicable boundary conditions as follows Abbas et al.[35]

$$\begin{aligned} &u_1 = u_{1_w} = bX^{\frac{1}{3}},\ u_2 = -u_{2_w},\ \mathrm{T} = \mathrm{T}_w,\ C = C_w \quad at \quad Y = 0 \\ &C \to C_\infty,\ u_1 \to 0,\ \mathrm{T} \to \mathrm{T}_\infty \qquad as \quad Y \to \infty \end{aligned} \tag{5}$$

According to $u_{2_w} = u_{2_0} X^{-\frac{1}{3}}$, the suction velocity u_{2_w} is thought to change with the X-coordinate. Using the following transformations, the governing equations are reduced to their non-dimensional form.

$$\begin{aligned} &\xi = \frac{1}{X^{\frac{1}{3}}}\sqrt{\frac{b}{u_{2_f}}}Y,\ u_1 = b\,X^{\frac{1}{3}} g'(\xi),\ u_2 = -\frac{\sqrt{b\,u_{2_f}}}{3X^{\frac{1}{3}}}\left(2g(\xi) - \xi\, g'(\xi)\right), \\ &\theta(\xi) = \frac{\mathrm{T} - \mathrm{T}_\infty}{\mathrm{T}_w - \mathrm{T}_\infty},\ \chi(\xi) = \frac{C - C_\infty}{C_w - C_\infty} \end{aligned} \tag{6}$$

According to the following equations, it is assumed that the tangent hyperbolic ferrofluid's thermal conductivity (κ) changes with the dimensionless temperature θ.

$$\kappa = \kappa_\infty (1 + \lambda\theta) \tag{7}$$

Thermophysical properties of hybrid ferroparticles is defined by

$$\left.\begin{aligned} &\left(\rho C_p\right)_{Hnf} = (1-\phi_{s2})\left[(1-\phi_{s1})\left(\rho C_p\right)_{fl} + \phi_{s1}\left(\rho C_p\right)_{s1}\right] + \phi_{s2}\left(\rho C_p\right)_{s2} \\ &\rho_{Hnf} = (1-\phi_{s2})\left[(1-\phi_{s1})\rho_{fl} + \phi_{s1}\rho_{s1}\right] + \phi_{s2}\rho_{s2}, \\ &\frac{\sigma_{Hnf}}{\sigma_{fer}} = \frac{\sigma_{s2} + 2\sigma_{fer} - 2\phi_{s2}\left(\sigma_{fer} - \sigma_{s2}\right)}{\sigma_{s2} + 2\sigma_{fer} + \phi_{s2}\left(\sigma_{fer} - \sigma_{s2}\right)}, \frac{\sigma_{fer}}{\sigma_{fl}} = \frac{\sigma_{s1} + 2\sigma_{fl} - 2\phi_{s1}\left(\sigma_{fl} - \sigma_{s1}\right)}{\sigma_{s1} + 2\sigma_{fl} + \phi_{s1}\left(\sigma_{fl} - \sigma_{s1}\right)}, \\ &\mu_{Hnf} = \frac{\mu_{fl}}{(1-\phi_{s1})^{2.5}(1-\phi_{s2})^{2.5}}, \end{aligned}\right\} \tag{8}$$

Table 1: Thermophysical characteristics corresponding to the base fluids and ferroparticles.

Physical properties	ρ **(kg/m^3)**	σ **(S/m)**	C_p **(J/kg· K)**
Cobalt ferrite ($CoFe_2O_4$)	4907	$1.1\text{x}10^{7}$	700
Magnetite (Fe_3O_4)	5180	$0.74\text{x}10^{6}$	670
Water (H_2O)	997	$5.5\text{x}10^{-6}$	4179

The non-dimensional equations:

$$\frac{A_{11}}{A_{12}}\left[(1-p)+pW_e g''\right]g'''-\left(\frac{1}{3}+Da_p\right)g'^2-\frac{1}{A_{12}}\left(LA_{13}+\beta_p A_{11}\right)g'+\frac{2gg''}{3}+G_r\theta+G_m\chi=0 \quad (9)$$

$$\chi''+Sc\frac{2}{3}g\chi'+\frac{\omega_b}{\omega_t}\theta''-Sc\alpha\chi=0 \quad (10)$$

$$A_{14}\frac{1}{\mathrm{P}_r}\left((1+R_d)(1+\lambda\theta)\theta''+\lambda\theta'^2\right)+\omega_b\phi'\theta'+\omega_t\theta'^2+\frac{2}{3}g\theta'+\frac{A_{11}}{A_{14}}E_c\left[(1-p)g''^2+\frac{p}{2}W_e g''^3\right]+A_{14}Q_1\theta=0 \quad (11)$$

With the boundary conditions:

$$\begin{aligned} &g=g_w,\quad g'=1,\quad \theta=1,\ \chi=1,\quad at\quad \xi=0,\\ &g'=0,\quad \theta=0,\quad \chi=0\quad as\quad \xi\to\infty \end{aligned} \quad (12)$$

The dimensionless variables are:

$$\beta_p=\frac{u_{2_{fl}}X^{\frac{2}{3}}}{bK},\ g_w=\frac{3u_{2_0}}{2\sqrt{bu_{2_{fl}}}},\ L=\frac{\sigma_{fl}M_0^2}{b\rho_{fl}},\ W_e=\frac{\sqrt{2}b^{\frac{3}{2}}X\Gamma}{\sqrt{u_{2_{fl}}}},\ E_c=\frac{u_{1_w}{}^2}{C_p\left(\mathrm{T}_w-\mathrm{T}_\infty\right)},R_d=\frac{16\sigma^*\mathrm{T}_\infty^3}{3k^*\kappa}$$

$$G_r=\frac{g\beta u_{2_{fl}}X^{\frac{1}{3}}\left(\mathrm{T}_w-\mathrm{T}_\infty\right)}{b^2},\ G_m=\frac{g\beta^* u_{2_{fl}}X^{\frac{1}{3}}\left(C_w-C_\infty\right)}{b^2},\ Da_p=\frac{\zeta_f}{\sqrt{K}}x,\ \mathrm{P}_r=\frac{\mu_f C_{Pfl}}{\kappa_\infty}, \quad (13)$$

$$\omega_t=\tau N_B\frac{\left(\mathrm{T}_w-\mathrm{T}_\infty\right)}{\nu},\ \delta_c=\frac{\tau N_T}{\mathrm{T}_\infty}\frac{\left(C_w-C_\infty\right)}{\nu},\ Sc=\frac{\nu}{N_B},\ \alpha=\frac{KX^{\frac{2}{3}}}{b},\ Q_1=\frac{QX^{\frac{2}{3}}}{b\left(\rho C_p\right)_{fl}}$$

Other essential parameters governing the flow are, the local heat transfer rate, the Shear drag coefficient and the local Sherwood number is,

$$\mathrm{Re}_X^{-1/2}Nu_X=-\theta'(0),\mathrm{Re}_X^{1/2}Cf_X=-\left[(1-p)g''(0)+\frac{pW_e}{2}g''^2(0)\right],\quad \mathrm{Re}_X^{-1/2}Sh_X=-\chi'(0) \quad (14)$$

Where, $\mathrm{Re}_X=\frac{u_{1_w}X}{u_{2_{fl}}}$ is the local flow Reynolds number.

The governing equations together with corresponding non-dimensional boundary conditions are defined by equations (9)–(11). MATLAB's bvp4c is employed to obtain numerical solutions of first-order ODEs obtained from transforming the initial linear ordinary differential equations. The following presumptions govern how the analysis is conducted:

$$g = y_1,\quad g' = y_2,\quad g'' = y_3,\quad \theta = y_4,\quad \theta' = y_5,\quad \chi = y_6,\quad \chi' = y_7 \tag{15}$$

The following is the derivation of the first-order differential equations from the nonlinear differential equation system:

$$yy1 = \frac{\left(\frac{1}{3} + Da_p\right) y_2{}^2 + \frac{1}{A_{12}}\left(LA_{13} + \beta_p A_{11}\right) y_2 - \frac{2y_1 y_3}{3} - G_r y_4 - G_m y_6}{\frac{A_{11}}{A_{12}}\left[(1-p) + pW_e y_3\right]} \tag{16}$$

$$yy3 = -Sc\frac{2}{3} y_1 y_7 - \frac{\omega_b}{\omega_t} yy2 + Sc\alpha y_6 \tag{17}$$

$$yy2 = \frac{1}{(1+R_d)(1+\lambda y_4)}\left(\frac{-\omega_b y_5 y_7 - \omega_t y_5{}^2 - \frac{2}{3} y_1 y_5 - \frac{A_{11}}{A_{14}} E_c\left[(1-p) y_3{}^2 + \frac{p}{2} W_e y_3{}^3\right] - A_{14} Q_1 y_4}{\frac{A_{14}}{\mathrm{P}_r}} - \lambda y_5{}^2\right) \tag{18}$$

$$y_1(0) = g_w,\quad y_2(0) = 1,\quad y_4(0) = 1,\quad y_6(0) = 1,$$
$$y_2 \to 0,\quad y_4 \to 1,\quad y_6 \to 1 \ as \ \ \xi \to \infty$$

RESULTS AND DISCUSSIONS

MATLAB's bvp4c solver and the shooting strategy are utilized to numerically determine the solutions of the nonlinear ODEs (9)–(11) along with the associated boundary conditions (12). Graphs 2–21 show and explain how different physical factors influence the concentration, temperature and velocity distributions. The numerical results of the physical coefficients are shown in Table 3. A comparison of the current We-values with those previously published by Abbas et al.[35] is shown in Table 4.

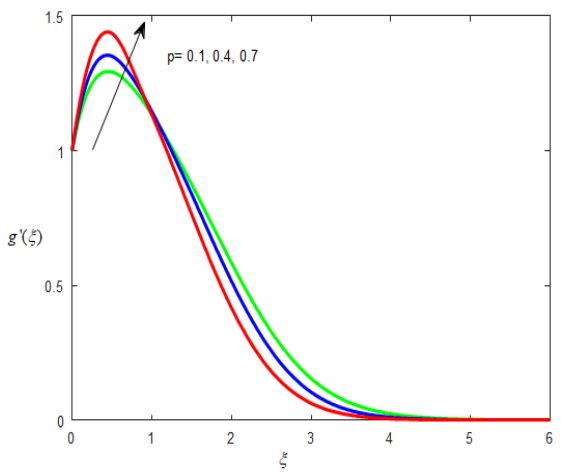

Figure 2.

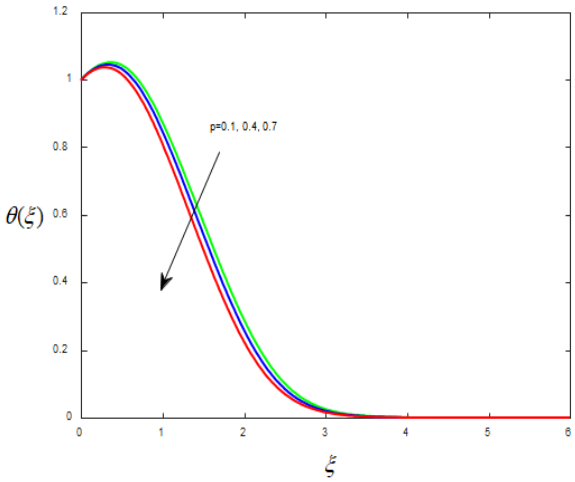

Figure 3.

The variation in temperature and velocity profiles with respect to the power-law index (p) is presented in graphs 2&3. When p increases lead to a rise in the velocity profile and enhances fluid deformation because it enlarges the momentum boundary layer. Greater p values cause the sheet to stretch more forcefully, which improves the fluid's downward flow. However, when p rises, the temperature profile falls, suggesting better heat transport and a matching decrease in the thickness of the thermal barrier layer. Additionally, for increasing p values, the velocity within the boundary layer decreases, indicating that the fluid gets greater resistance to shear pressures. This decrease in velocity is accompanied by improved fluid stretching and more effective heat transfer, underscoring the power-law index's dual impact on momentum and thermal transport properties.

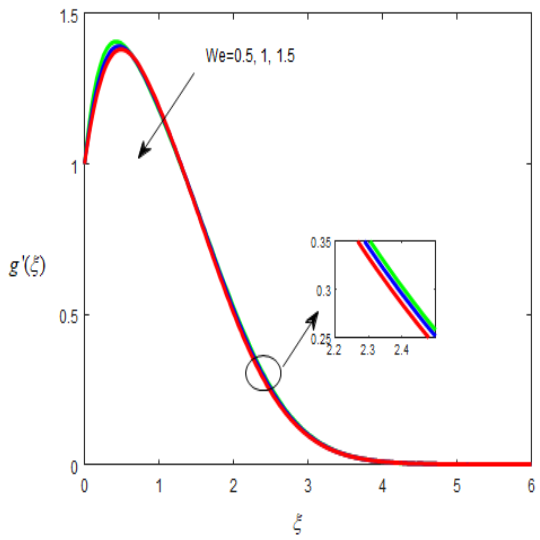

Figure 4.

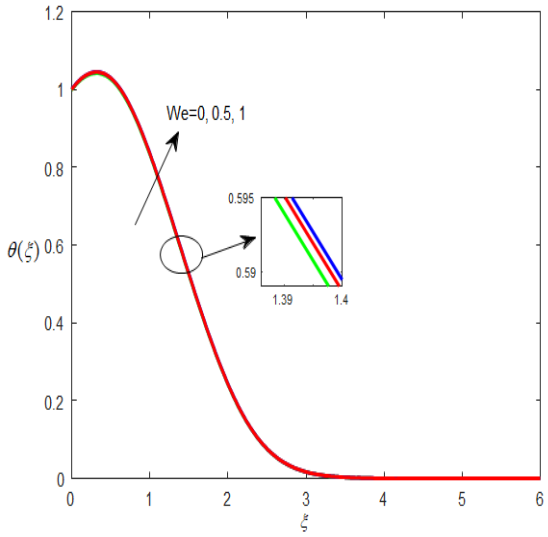

Figure 5.

The variation of the ferrofluid's velocity and temperature profiles with respect to Weissenberg number (We) can be observed in Figures 4 and 5. The fluid velocity falls as We rises, suggesting that the fluid is more resistant to deformation and takes longer to react to the applied flow. In contrast, higher values of We correspond to an enhanced temperature profile, indicating more thermal energy in the boundary layer. Greater values indicate a slower fluid reaction to external forces. The Weissenberg number quantifies the ratio of the relaxation time of the fluid to the characteristic time scale of the flow. As (We) grows, this explains the observed decrease in velocity and the corresponding rise in temperature.

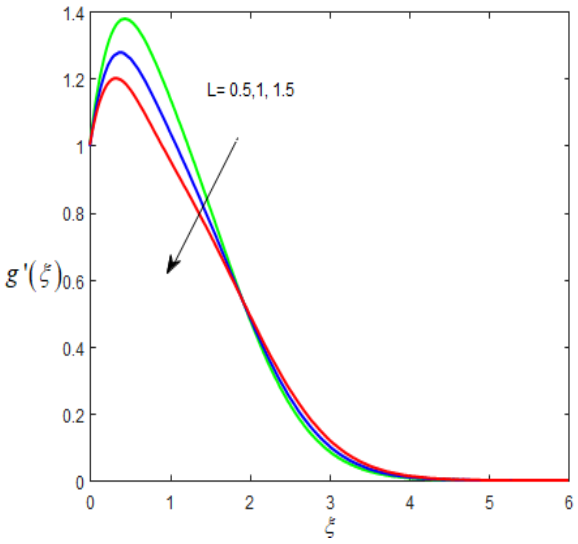

Figure 6.

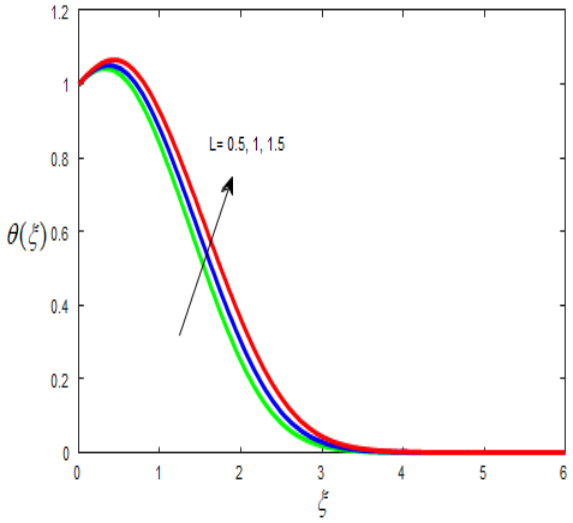

Figure 7.

Graphs 6 & 7 display how the ferrofluid's velocity and temperature distributions are impacted by the magnetic field(L). With higher values of L, the amplified Lorentz force resisting the fluid's motion leads to a considerable decrease in velocity.. The temperature distribution, on the other hand, shows an upward trend as L increases, suggesting that the boundary layer has more thermal energy. In the physical world, greater magnetic fields encourage thermal transfer in the ferrofluid while suppressing momentum transmission. Applications in engineering and biomedicine, such as magnetic drug targeting, ferrofluid-based heat exchangers, and cooling technologies, where exact control over flow resistance and heat transfer is essential, greatly benefit from such behavior.

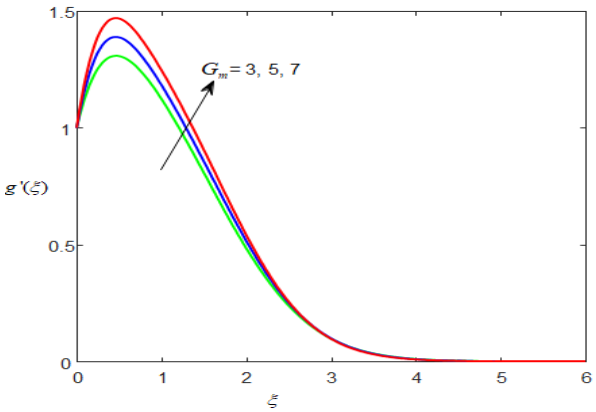

Figure 8.

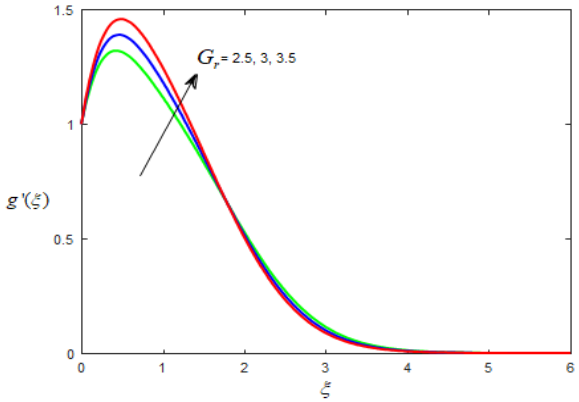

Figure 9.

The impact of Grashof numbers, both solutal (Gm) and thermal (Gr) on ferrofluid flow properties are shown in Figures 8 and 9. By increasing buoyant forces in relation to viscous

resistance, both factors are shown to improve fluid motion. Enhanced thermal Grashof number (Gr) amplify free convection and speed up fluid motion within the boundary layer It indicates the proportion of thermal buoyancy versus viscous forces. Likewise, concentration-driven buoyancy effects are represented by the solutal Grashof number (Gm), where greater values encourage stronger fluid acceleration close to the sheet. Consequently, As Gr and Gm increase, the momentum boundary layer thins, suggesting that buoyant forces are stronger than viscous effects. Larger Gr and Gm typically lead to enhanced convective transport and changed boundary layer dynamics in the ferrofluid system, which is especially important for applications like separation technologies, chemical processing, and thermal management.

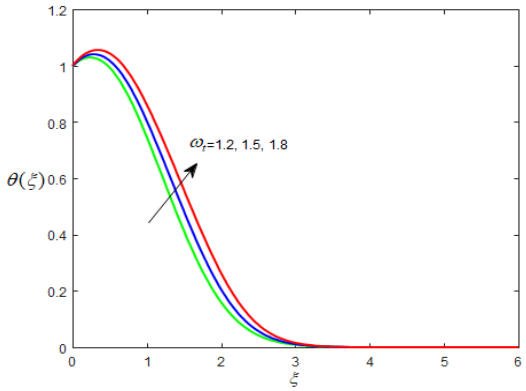

Figure 10.

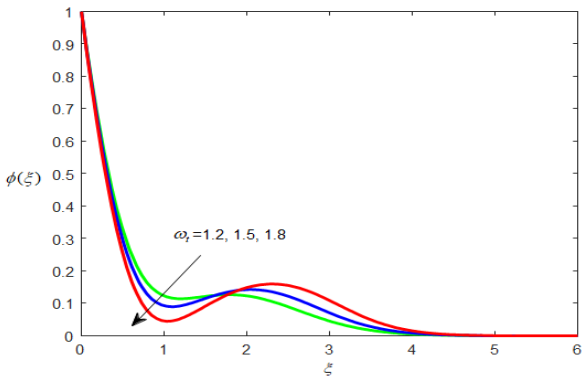

Figure 11.

Figures 10 and 11 depict how the thermophoretic factor (ω_t) influences the ferrofluid's temperature and concentration distributions. As ω_t grows, the increase in boundary layer temperature leads to a thicker thermal boundary layer because of stronger thermal transport. However, because thermophoretic forces drive nanoparticles toward cooler regions and away from hotter regions, the concentration profile falls as ω_t increases. This suggests that thermophoresis has two functions: it improves heat transport and reduces the fluid's concentration of nanoparticles. These effects are significant in real-world applications where particle distribution and heat transfer efficiency are crucial, such as solar energy collectors and cooling devices based on nanofluids.

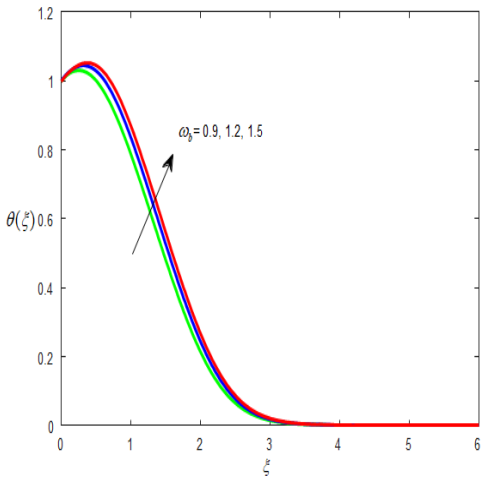

Figure 12.

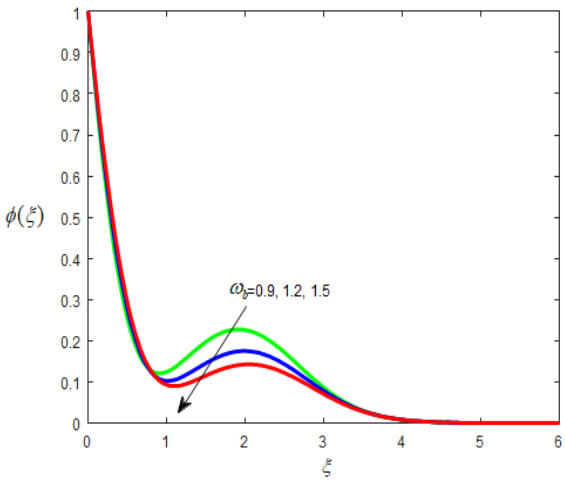

Figure 13.

Figures 12 and 13 show how the ferrofluid's temperature and concentration profiles are affected by the Brownian diffusion factor (ω_b). As the nanoparticles exhibit greater random mobility promotes better heat transfer and a higher thermal profile, it has been observed that increasing ω_b raises thermal energy in the fluid. On the other hand, larger ω_b values encourage more dispersion of nanoparticles, which lowers the local concentration inside the boundary layer. The dual function of Brownian motion in increasing heat transfer and decreasing nanoparticle concentration is highlighted by this behaviour. This feature is especially significant in applications like biomedical fluid transport and microelectronics cooling.

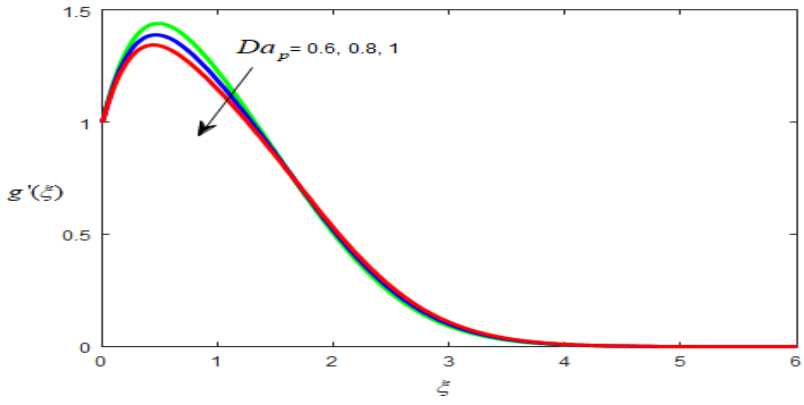

Figure 14.

Figure 14 shows how the velocity distribution of the ferrofluid is affected by the Darcy–Forchheimer parameter Da_p. Resistance and friction against the flow rise as Da_p increases, taking into consideration the impact of local inertial forces inside the porous medium. The

outcome is a sharp decrease in fluid velocity and momentum, and an increase in flow resistance results in momentum barrier layer to thin. Used in geothermal energy applications, filtration procedures and packed-bed reactors, this behaviour highlights the crucial role that the parameter Da_p plays in managing the transfer of momentum and fluid dynamics inside porous media.

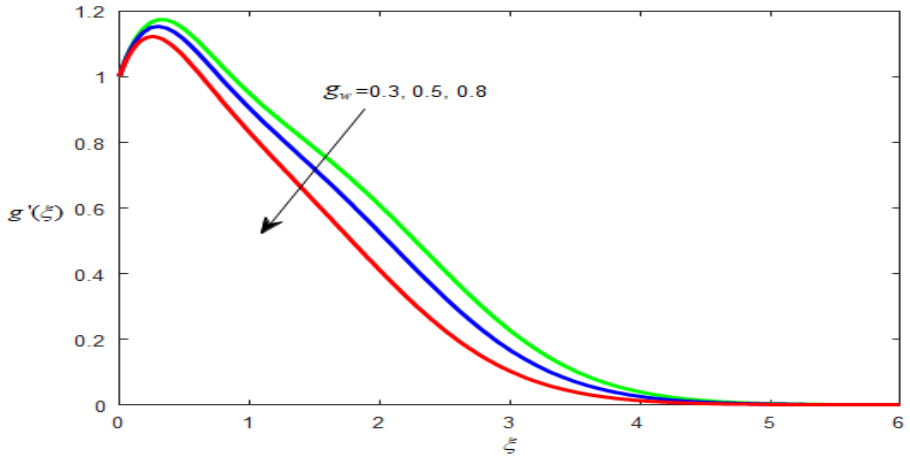

Figure 15:

The significance of the suction factor g_w on the ferrofluid's velocity distribution is shown in figure 15. The findings indicate that the fluid's velocity falls with increasing g_w, particularly at larger values. This occurs because increased resistance caused by stronger suction through the porous surface slows down the flow. In essence, the suction parameter indicates the rate at which fluid passes through the porous medium. The fluid loses momentum and the flow weakens as this rate rises. This decrease in velocity demonstrates how suction may be very important in regulating fluid dynamics and forming the boundary layer in porous materials. These effects are especially significant in a variety of filtration procedures and better oil recovery in petroleum engineering.

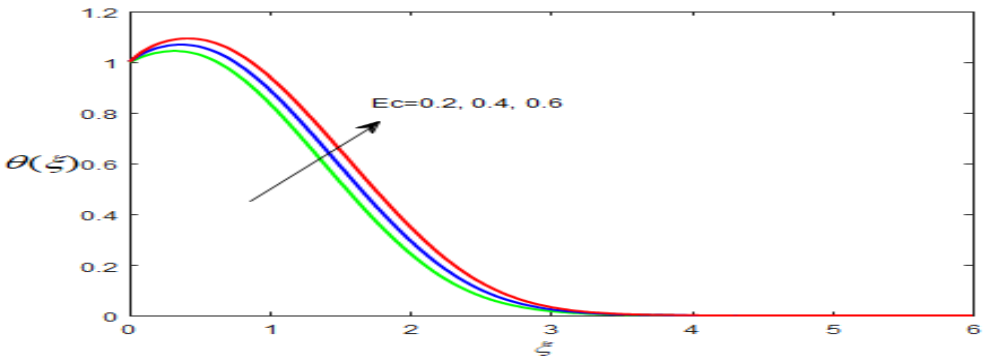

Figure 16.

Figure 16 shows how the temperature profile responds to changes in the Eckert number Ec. The Eckert number, which measures viscous dissipation effects in the flow, is defined as the kinetic-to-thermal energy ratio. Frictional heating causes some of the flow's kinetic energy to transform into internal energy, which intensifies as Ec rises. The temperature distribution is raised by this extra heating, which also causes a larger thermal boundary layer throughout the area. The results clearly show that higher values of Ec increase the thermal behaviour of the ferrofluid by amplifying the influence of viscous dissipation. These effects are important in real-world settings where viscous heating cannot be disregarded, such as microchannel heat exchangers, lubrication procedures, and high-speed thermal systems.

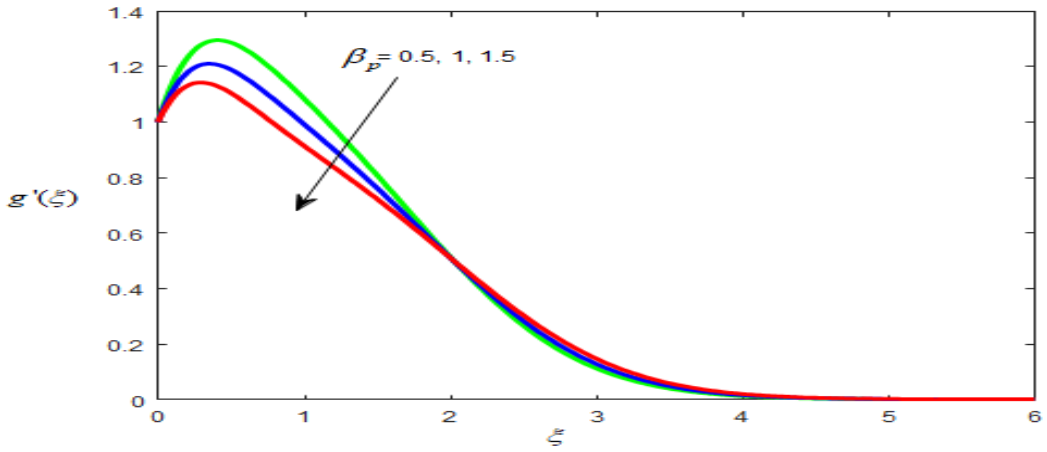

Figure. 17.

Figure 17 shows how the ferrofluid's velocity profile is affected by the porosity parameter β_p. It has been found that as β_p increases, fluid velocity decreases because the medium's increased porosity or decreased permeability creates a greater resistance to motion. By impeding fluid movement, the extra friction produced inside the porous structure slows down the ferrofluid and thins the momentum boundary layer. This displays the porosity parameter's governing function in controlling flow resistance and velocity distribution. In technical applications involving porous media, such catalytic reactors, geothermal energy extraction, and groundwater filtering, these effects are very important.

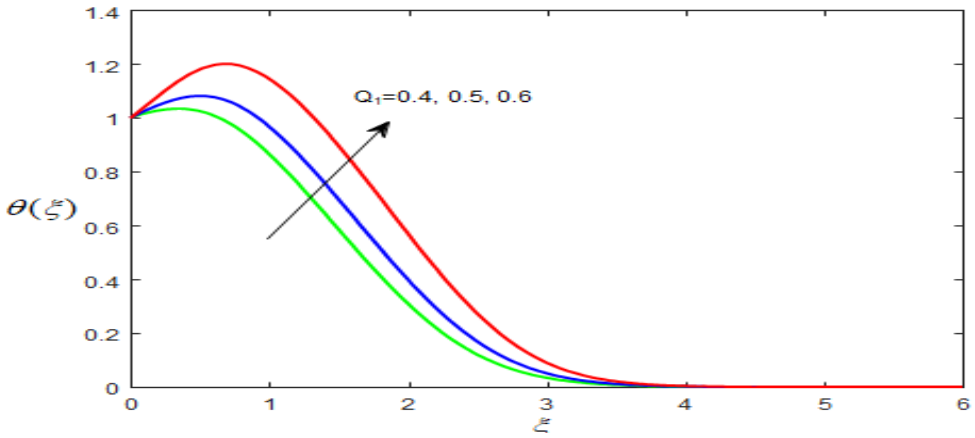

Figure 18.

Figure 18 shows how the ferrofluid's temperature gradient is affected by heat generation parameter Q_1. When Q_1 rises, supplying more heat to the system leads to an enhanced heat content in the boundary layer. As a result thermal boundary layer expands and the dimensionless temperature profile θ(η) rises. The fluid can retain more heat and enlarge the border region when an external heat source is present because it amplifies the temperature gradient. All things considered, higher values of Q_1 greatly raise the fluid temperature. These effects are practically important for systems that generate or absorb heat like nuclear power plants, energy storage systems and electronic cooling devices.

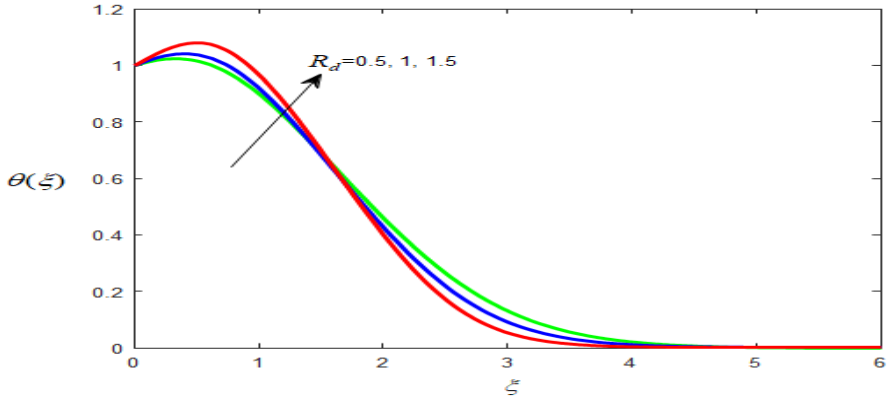

Figure 19.

Figure 19 illustrates the variation in the ferrofluid's temperature profile under the influence of radiation parameter R_d . The temperature boundary layer thickness grows with higher radiative energy transfer, causing the temperature in the boundary layer to rise with an increase in R_d . Greater magnitudes of R_d raise the temperature distribution even further by increasing the heat absorbed by the fluid and decreasing the mean absorption coefficient. This

impact can also be enhanced by the application of a magnetic flux. These findings demonstrate how radiation shows a major role in heat transmission, showing that greater radiation parameters amplify temperature profiles and widen the thermal boundary layer.

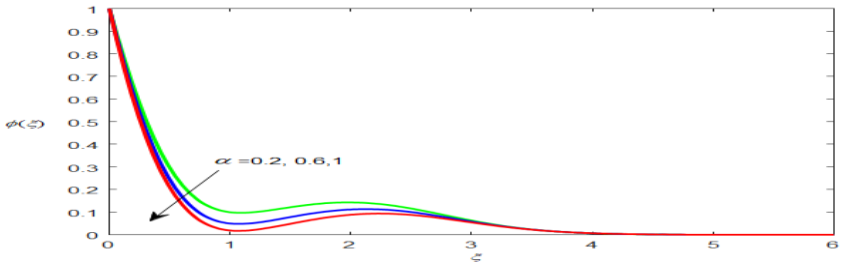

Figure 20.

Figure 20 shows how the ferrofluid's concentration field is affected by changes in the chemical reaction rate parameter α. The study confirms that the concentration of ferroparticles falls with increasing α, creating a smaller concentration boundary layer. Higher α values physically accelerate the rate of harmful chemical reactions that consume nanoparticles and lower their concentration locally. Although the influence of the chemical reaction parameter on temperature and velocity distributions is minimal, it significantly changes the distribution of concentrations. This suggests that chemical reactions are the main mechanism governing the concentration of nanoparticles in the boundary layer. Increased α values decrease the thickness of the boundary layer and the magnitude of the concentration while essentially ignoring the flow and temperature fields. These effects are significant in chemical reactors, catalytic systems, and medicinal drug delivery applications, among other processes requiring reactive nanofluids.

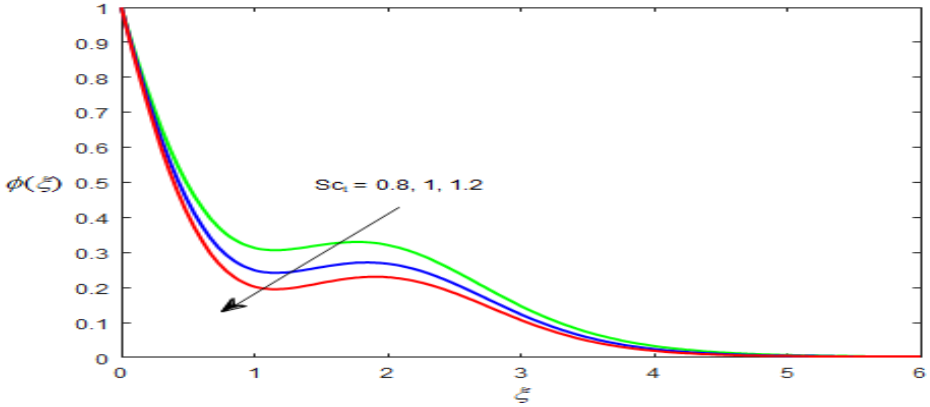

Figure 21.

Figure 21 shows how the ferrofluid's concentration profile is affected by the Schmidt number (Sc_t). It is found that the concentration of ferroparticles falls with increasing Sc_t, leading to a narrower solutal boundary layer. Greater Sc_t values translate into lower Brownian diffusivity because momentum diffusivity in relation to mass diffusivity is expressed by the dimensionless Schmidt number. This decrease in diffusivity weakens the concentration profile by limiting the nanoparticles tendency to diffuse further within the fluid. Higher Sc_t fluids consequently show less nanoparticle mobility and reduced depth of penetration, both of which result in a reduction of the temperature profile. In general, rising Sc_t decreases boundary layer's concentration and temperature profiles, underscoring its crucial function in controlling mass and heat transport.

Table 2.

L	β_p	p	We	Da_p	Gm	Gr	Sc_t	α	Cf	Sh
0	0.5	0.1	0.5	0.2	0.1	0.2	2.01	0.1	0.893106	1.155741
0	0.5	0.1	0.5	0.4	0.1	0.4	2.01	0.1	0.948417	1.182186
0.5	0.5	0.1	0.5	0.6	0.1	0.6	2.01	0.1	0.845424	1.200222
0.5	0.0	0.1	0.5	0.2	0.3	0.2	2.01	0.1	0.898211	1.182861
0.5	0.0	0.1	0.5	0.4	0.3	0.4	2.01	0.1	0.953522	1.215286
0.5	0.0	0.1	0.5	0.6	0.3	0.6	2.01	0.1	1.008834	1.247712
0.5	0.1	0.2	0.2	0.2	0.3	0.2	2.01	0.2	0.903231	1.199621
1.0	0.1	0.2	0.2	0.4	0.5	0.4	2.01	0.2	0.881827	1.246196
1.0	0.1	0.2	0.2	0.6	0.5	0.6	2.01	0.2	0.937139	1.284602
1.0	1.0	0.3	0.1	0.2	0.5	0.2	2.01	0.2	0.670386	1.180961
1.0	1.0	0.3	0.1	0.4	0.5	0.4	2.01	0.2	0.725697	1.219366
1.0	1.0	0.3	0.1	0.6	0.1	0.6	2.01	0.2	0.635409	1.200692

Table 2 displays the effects of various governing parameters on the skin friction and Sherwood number. An overview of how these parameters influence the transport characteristics is given in the table. Increasing the power-law index, porosity parameter, and weissenberg number results in lower values of the sherwood number along with the coefficient of skin friction. On the other hand, these quantities are enhanced by greater solutal and thermal Grashof numbers, suggesting stronger buoyancy-driven effects. Surface drag is decreased during magnetic field interaction because this leads to the development of a Lorentz force that opposes fluid motion. Moreover, the sherwood number decreases with rising values of both the schmidt number and the chemical reaction parameter, which also raise skin friction.

Table 3: Assessment of Skin friction against previously findings of Abbas and co-author,[35] when L=p=0.2 and $Da_p = \beta_p = G_m = G_r = g_w = 0$.

We	Present study	Abbas et al.[35]
0.5	0.7796041	0.779623
1.0	0.8520821	0.852030
2.0	0.7859603	0.785905

CONCLUSIONS

- As the power-law index rises, velocity increases but temperature decreases because of increased heat transfer.
- Through relaxing effects, a higher Weissenberg number raises temperature while decreasing fluid velocity.
- Through Lorentz effects, the magnetic parameter reduces velocity while raising thermal energy in the boundary layer.
- The buoyancy forces are increased by thermal and solutal Grashof numbers, which speed up flow and thin the momentum boundary layer.
- The thermophoretic parameter drives particles away from hot areas, increasing temperature while decreasing nanoparticle concentration.
- By increasing dispersion, Brownian motion reduces nanoparticle concentration while improving heat transmission.
- Both suction and the Darcy–Forchheimer parameter decrease velocity by adding more resistance to porous medium.
- The Eckert number thickens the thermal boundary layer by increasing temperature through viscous dissipation.
- The thermal boundary region is expanded and the temperature is further raised by heat generation and radiation parameters.
- The chemical reaction parameter lowers the concentration of nanoparticles without significantly changing temperature or velocity.
- As diffusivity decreases with a larger Schmidt number, concentration and temperature profiles become weaker.

REFERENCES

1. K. Javaherdeh, M. Mirzaei Nejad, and M. Moslemi, Natural convection heat and mass transfer in MHD fluid flow past a moving vertical plate with variable surface temperature

and concentration in a porous medium, *Engineering Science and Technology, an International Journal*, Sep. 2015; 1(3): 423–431, doi: 10.1016/j.jestch.2015.03.001.

2. B. Zigta, Effect of thermal radiation and chemical reaction on mhd flow of blood in stretching permeable vessel, *International Journal of Applied Mechanics and Engineering*, Aug. 2020; 25(3): 198–211, doi: 10.2478/ijame-2020-0043.
3. S. Nasir and A. S. Berrouk, Numerical investigation of chemical reactive MHD fluid dynamics over a porous surface with Cattaneo–Christov heat flux, *J Therm Anal Calorim*, Dec. 2024; 149(24): 14877–14900, doi: 10.1007/s10973-024-13815-z.
4. R. A. Mohamed, Double-Diffusive Convection-Radiation Interaction on Unsteady MHD Flow over a Vertical Moving Porous Plate with Heat Generation and Soret Effects, 2014. [Online]. Available: https://www.researchgate.net/publication/228767047
5. B. M. Cham, S. ul Islam, A. H. Majeed, M. R. Ali, and A. S. Hendy, Numerical computations of magnetohydrodynamic (MHD) thermal fluid flow in a permeable cavity: A time dependent based study, *Case Studies in Thermal Engineering*, Sep. 2024; 61: doi: 10.1016/j.csite.2024.104905.
6. M. Khan, M. Y. Malik, T. Salahuddin, and A. Hussian, Heat and mass transfer of Williamson nanofluid flow yield by an inclined Lorentz force over a nonlinear stretching sheet, *Results Phys*, Mar. 2018; 8: 862–868, doi: 10.1016/j.rinp.2018.01.005.
7. N. S. Akbar, A. Al-Zubaidi, S. Saleem, and S. A. M. Alsallami, Variable fluid properties analysis for thermally laminated 3-dimensional magnetohydrodynamic non-Newtonian nanofluid over a stretching sheet, *Sci Rep.*, Dec. 2023; 13(1): doi: 10.1038/s41598-023-30233-7.
8. B. Prabhakar Reddy and O. D. Makinde, Numerical study on MHD radiating and reacting unsteady slip flow past a vertical permeable plate in a porous medium, *International Journal of Ambient Energy*, 2022; 43(1): 6007–6016, doi: 10.1080/01430750.2021.1999323.
9. N. Mami and M. N. Bouaziz, Effect of MHD on nanofluid flow, heat and mass transfer over a stretching surface embedded in a porous medium, *Periodica Polytechnica Mechanical Engineering*, Mar. 2018; 62(2): 91–100, doi: 10.3311/PPme.10622.
10. M. Santhi, K. V. Suryanarayana Rao, P. Sudarsana Reddy, and P. Sreedevi, Heat and mass transfer characteristics of radiative hybrid nanofluid flow over a stretching sheet with chemical reaction, *Heat Transfer*, May 2021; 50(3): 2929–2949, doi: 10.1002/htj.22012.

11. D. Khan, K. K. Asogwa, T. Alqahtani, S. Algarni, S. Alqahtani, and M. A. Akbar, A Generalized Two-Phase Free Convection Flow of Dusty Jeffrey Fluid between Infinite Vertical Parallel Plates with Heat Transfer, *Journal of Mathematics*, 2022; 2022, doi: 10.1155/2022/8470139.
12. P. R. Sekhar, S. Sreedhar, S. M. Ibrahim, and P. V. Kumar, Radiative Heat Source Fluid Flow of MHD Casson Nanofluid over A Non-Linear Inclined Surface with Soret and Dufour Effects, *CFD Letters*, Jul. 2023; 15(7): 42–60, doi: 10.37934/cfdl.15.7.4260.
13. M. Khan, A. Hussain, M. Y. Malik, T. Salahuddin, and F. Khan, Boundary layer flow of MHD tangent hyperbolic nanofluid over a stretching sheet: A numerical investigation, *Results Phys.*, 2017; 7: 2837–2844, doi: 10.1016/j.rinp.2017.07.061.
14. A. Kotnurkar and S. Gowda, Influence of magnetic field and activation energy on creeping flow of tri-hybrid nanofluid driven by peristaltic pumping in an asymmetric channel with synthetic cilia, *Discover Mechanical Engineering*, Dec. 2024; 3(1), doi: 10.1007/s44245-024-00074-3.**0**
15. Z. Mahmood *et al.*, Heat transfer in radiative hybrid nanofluids over moving sheet with porous media and slip conditions: Numerical analysis of variable viscosity and thermal conductivity, *Mater Today Commun*, Aug. 2024; 40, doi: 10.1016/j.mtcomm.2024.109664.
16. H. A. Madkhali, M. Ahmed, M. Nawaz, S. O. Alharbi, A. S. Alqahtani, and M. Y. Malik, Numerical study on the role of ternary nanoparticles on heat transfer enhancement in MHD flow of cross-rheological-fluid, *Case Studies in Thermal Engineering*, Nov. 2023; 51, doi: 10.1016/j.csite.2023.103579.
17. A. M. Alqahtani, M. Bilal, F. A. Aziz Elsebaee, S. M. Eldin, T. R. Alsenani, and A. Ali, Energy transmission through carreau yasuda fluid influenced by ethylene glycol with activation energy and ternary hybrid nanocomposites by using a mathematical model, *Heliyon*, Apr. 2023; 9(4): doi: 10.1016/j.heliyon.2023.e14740.
18. N. Elboughdiri *et al.*, Numerical simulation of Stephan blowing impacts on thermally laminated 3D flow of MHD trihybrid nanofluid with Soret and Dufour effects, *Case Studies in Thermal Engineering*, Feb. 2025; 66, doi: 10.1016/j.csite.2024.105460.
19. S. Ahmad and S. Nadeem, Analysis of activation energy and its impact on hybrid nanofluid in the presence of Hall and ion slip currents, *Applied Nanoscience (Switzerland)*, Dec. 2020; 10(12): 5315–5330, doi: 10.1007/s13204-020-01334-w.
20. D. S. Dzhuraev and M. M. Safarov, Studies of Thermophysical Properties of Ferrofluids, *Measurement Techniques*, Oct. 2016; 59(7): 743–746, doi: 10.1007/s11018-016-1040-z.

21. Z. Mahmood *et al.*, Deep learning investigation of water-based tetra hybrid nanofluid across a shrinking cylinder for variable electrical conductivity with thermal radiation, *J Radiat Res Appl Sci.*, Mar. 2025; 18(1): 101213, doi: 10.1016/j.jrras.2024.101213.
22. Z. Mahmood *et al.*, Analysis of heat generation and viscous dissipation with thermal radiation on unsteady hybrid nanofluid flow over a sphere with double-stratification: Case of modified Buongiorno's model, *J Radiat Res Appl Sci.*, Dec. 2024; 17(4): 101146, doi: 10.1016/j.jrras.2024.101146.
23. H. T. Alkasasbeh, Numerical Solution of Heat Transfer Flow of Casson Hybrid Nanofluid over Vertical Stretching Sheet with Magnetic Field Effect, *CFD Letters*, Mar. 2022; 14(3): 39–52, doi: 10.37934/cfdl.14.3.3952.
24. N. S. Wahid, N. Md Arifin, N. S. Khashi'ie, I. Pop, N. Bachok, and M. E. H. Hafidzuddin, MHD mixed convection flow of a hybrid nanofluid past a permeable vertical flat plate with thermal radiation effect, *Alexandria Engineering Journal*, Apr. 2022; 61(4): 3323–3333, doi: 10.1016/j.aej.2021.08.059.
25. U. Yashkun, K. Zaimi, N. A. Abu Bakar, A. Ishak, and I. Pop, MHD hybrid nanofluid flow over a permeable stretching/shrinking sheet with thermal radiation effect, *Int J Numer Methods Heat Fluid Flow*, Mar. 2021; 31(3): 1014–1031, doi: 10.1108/HFF-02-2020-0083.
26. K. Sharma, N. Vijay, D. Bhardwaj, and R. Jindal, Flow of water conveying Fe3O4 and Mn–ZnFe2O4 nanoparticles over a rotating disk: Significance of thermophoresis and Brownian motion, *J Magn Magn Mater*, May 2023; 574: doi: 10.1016/j.jmmm.2023.170710.
27. K. Anantha Kumar, N. Sandeep, V. Sugunamma, and I. L. Animasaun, Effect of irregular heat source/sink on the radiative thin film flow of MHD hybrid ferrofluid, *J Therm Anal Calorim*, Feb. 2020; 139(3): 2145–2153, doi: 10.1007/s10973-019-08628-4.
28. M. M. Magdy, W. Abbas, K. S. Mekheimer, and M. S. Emam, Ferro-Fluid Flow and Heat Transfer over Unsteady Stretching Sheet in the Presence of a Nonuniform Magnetic Field, *Journal of Nonlinear Mathematical Physics*, Dec. 2025; 32(1), doi: 10.1007/s44198-024-00250-9.
29. L. F. Alharbi *et al.*, Heat transfer characteristics in a non-Newtonian (Williamson) hybrid nanofluid with Hall and convective boundary effects, *High Temperature Materials and Processes*, Jan. 2024; 43(1), doi: 10.1515/htmp-2024-0056.
30. M. V. Reddy, M. Ajithkumar, S. A. Lone, F. Ali, P. Lakshminarayana, and A. Saeed, Magneto-Williamson nanofluid flow past a wedge with activation energy: Buongiorno

model, *Advances in Mechanical Engineering*, Jan. 2024; 16(1), doi: 10.1177/16878132231223027.

31. S. Nadeem, S. T. Hussain, and C. Lee, FLOW OF A WILLIAMSON FLUID OVER A STRETCHING SHEET, 30(3): 619–625, [Online]. Available: www.abeq.org.br/bjche
32. W. Abbas, A. M. Megahed, and E. Fares, The impact of a chemical reaction on the heat and mass transfer mechanisms in a dissipative and radiative nanofluid flow over a nonlinear stretching sheet, *Sci Rep.*, Dec. 2024; 14(1), doi: 10.1038/s41598-024-57952-9.
33. S. Jagadeesh and M. C. K. Reddy, Convective Heat and Mass Transfer Rate on 3D Williamson Nanofluid Flow via Linear Stretching Sheet with Thermal Radiation and Heat Absorption, Sep. 02, 2022; doi: 10.21203/rs.3.rs-2005766/v1.
34. T. Hayat, Y. Saeed, S. Asad, and A. Alsaedi, Soret and Dufour effects in the flow of Williamson fluid over an unsteady stretching surface with thermal radiation, *Zeitschrift fur Naturforschung - Section A Journal of Physical Sciences*, 2015; 70(4): 235–243, doi: 10.1515/zna-2014-0252.
35. K. Rafique *et al.*, Numerical analysis of non-linear radiative Casson fluids containing CNTs having length and radius over permeable moving plate, *Open Physics*, Jan. 2024; 22(1), doi: 10.1515/phys-2024-0013.
36. N. Vijay and K. Sharma, Heat and mass transfer study of ferrofluid flow between co-rotating stretchable disks with geothermal viscosity: HAM analysis, *Chinese Journal of Physics*, Aug. 2022; 78: 83–95, doi: 10.1016/j.cjph.2022.05.014.
37. S. Mishra and H. Mondal, A Neuro-computational Proposal for the ZrO2-Fe3O4 Nanoparticles in the Engine Oil–based Hybrid Nanofluid, *Bionanoscience*, Dec. 2023, doi: 10.1007/s12668-023-01282-z.
38. K. Sharma, N. Vijay, D. Ram, and I. L. Animasaun, Significance of geothermal viscosity for the magnetic fluid flow between co-rotating porous surfaces, *Numeri Heat Transf A Appl.*, 2023; 84(9): 980–991, doi: 10.1080/10407782.2023.2167754.
39. S. Arulmozhi, K. Sukkiramathi, S. S. Santra, R. Edwan, U. Fernandez-Gamiz, and S. Noeiaghdam, Heat and mass transfer analysis of radiative and chemical reactive effects on MHD nanofluid over an infinite moving vertical plate, *Results in Engineering*, Jun. 2022; 14, doi: 10.1016/j.rineng.2022.100394.
40. K. Rafique, Z. Mahmood, Adnan, T. Muhammad, H. Alqahtani, and A. A. Shaaban, Dynamics of shape factor with Joule heating and thermal stratification on magnetohydrodynamic Al2O3-Cu-TiO2/H2O nanofluid of stretching disk: an

irreversibility analysis, *J Therm Anal Calorim*, Feb. 2024, doi: 10.1007/s10973-024-13269-3.